Frequency Switchable and Tunable Negative Group Delay Circuits Based on Defected Microstrip Structures

Chithra L. Palson[1, *], Rema K. Sreelal[2], Deepti D. Krishna[2], and Babita R. Jose[1]

Abstract—Group delay distortions are critical for high quality transmissions in today's communication system. In this paper, we have proposed the design and analysis of defected microstrip line-based Negative Group Delay Circuits (NGDCs) to compensate for group delay distortions. Initially, a tunable pulse shaped defection based NGD structure is designed wherein a variable resistor connection allows group delay tunability. The proposed design is able to generate a group delay (GD) tuning from 0 to -4.8 ns at 2.7 GHz as the resistance is varied from 1 kΩ to 1 MΩ. Further, we embedded two stubs to implement the switchable multi-band feature on the proposed NGDC design. The NGDCs are fabricated, and the measured results confirm the proposed concept. Lastly, we designed a tunable compact NGDC with inverted-U stubs inscribed inside a microstrip line. It generated GD tunability at different frequency bands with the aid of a variable resistor and switched the frequencies as required.

1. INTRODUCTION

For ideal linear phase filters, phase changes linearly with input signal frequency; hence, Group Delay (GD) should remain constant. But in reality, filters are nonlinear, and GD varies with frequency, often showing abnormal peaks at its passband/stopband transitions. GD gives a measure of the transmitted waveform distortion. Mathematically, it is the negative derivative of the transmission phase (S_{21}) with respect to frequency. If this rate of change is negative, it indicates a Positive Group Delay (PGD) and vice-versa for a Negative Group Delay (NGD). GD variations, which depend on the type of filters, increase with the filter order as well as decrease with the filter bandwidth. These would adversely change the shape of the output pulse resulting in Inter Symbol Interference (ISI). Therefore, signal processing techniques such as group delay equalization becomes necessary.

Clearly, PGD is the time lag of the signal envelope. However, it does not imply that NGD would mean a time advancement. Instead, it only means that the output pulse peak emerges outside the system before the input pulse peak enters the same. In other words, the system can predict its input wherever the group delay is negative without violating the principle of causality, and this super-luminal phenomenon would only reshape the signal [5]. Brillouin [6] found this NGD phenomenon in the 1960s inside the absorption band of a dispersive medium and further studied its super-luminal effects.

Recently, GD equalisation techniques utilising the NGD phenomenon [1–4] have attracted much attention. Since these NGD circuits (both passive and active) compensate for undesired PGD and improve phase linearity, they are utilised in various applications such as improving the efficiency of feed-forward amplifiers [7], reducing the beam squint delay in phased array antennas [8], minimising PGDs in circuits [9], bandwidth enhancement of feedback amplifier [10], improving the linearity and bandwidth of phase shifters [11, 12], and cancelling the time delays in sensors [13]. Typically in

microwave systems, GD is critical in the design of amplifiers, mixers, and filters. In such systems, NGD circuits can suppress undesired PGDs occurring within the operating frequency range. A detailed study on similarity between linear filter behaviour and NGD functions is illustrated, and eventually bandpass based NGD function is realized in [14]. Lately, there has been literature reported in the design of NGD circuits at microwave frequencies using periodic structures such as Defected Microstrip Structure (DMS) [15, 20, 23, 24], Defected Ground Structure (DGS) [16, 23] and Photonic BandGap (PBG) [17]. [20, 23, 24, 26] discuss multi-band NGDCs. [23] designs a dual band NGDC, and each of these bands is the resultant of the resistor connected DMS and DGS, respectively. [24] achieved a dual band NGDC with the aid of two U-shaped defections on the microstrip line. Tri-band NGDCs are realized in [20, 26] wherein [20] has GD tunability realized using three externally connected resistors. [25, 26, 28, 29, 31] propose NGDCs with low reflection losses.

Traditionally NGDC is a bandstop filter having an RLC resonator structure [18] primarily because it is generated at frequencies where signal attenuation is at its maximum. In the past few years, there have been several bandstop filter-based NGDC designs reported [19, 20]. However, only a few focus on the tunability of group delay [20–22]. In this paper, we propose compact and tunable transmission line-based NGDCs. Here, we utilise the stopband characteristics of DMS for 5G sub-6 GHz applications. Further, a general equivalent circuit model of NGDC is analysed, and the element parameters for each proposed circuit are extracted.

We started the NGDC design by loading a pulse-shaped stub in a rectangular defection made on a $50\,\Omega$ microstrip transmission line. A variable resistor is introduced in the circuit to alter the stopband attenuation and hence vary the GD. Two stubs loaded with RF switches are added to the pulse-shaped NGDCs to introduce the multi-band frequency switchability feature. The proposed designs are then fabricated, and the results are verified. Further, better performance is observed by replacing the pulse-shaped stub with two inverted U stubs inscribed in the microstrip line. The following sections discuss the designs, analysis, and observations.

2. PULSE-SHAPED STUB LOADED NGD CIRCUIT

Figure 1(a) shows the proposed single band NGDC on an FR4 substrate with a dielectric constant of 4.7 and height of 1.6 mm. It has a rectangular defection ($l_1 \times w_1$) inside the $50\,\Omega$ transmission line,
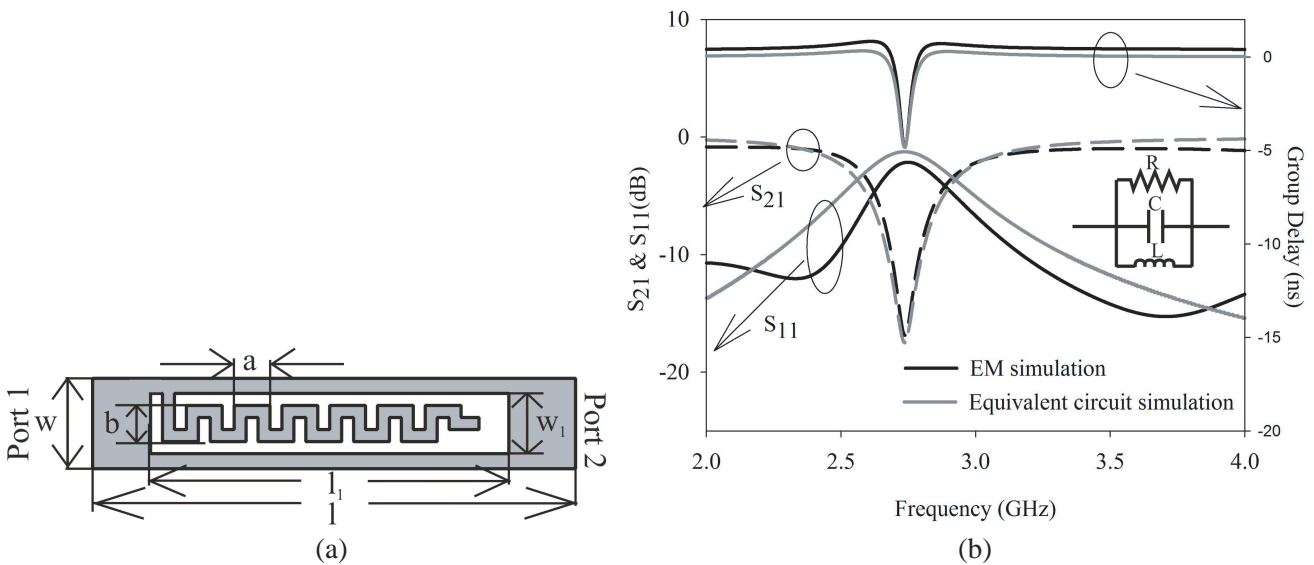
Figure 1. (a) Pulse-shaped stub loaded NGDC — $a = 1.2$, $b = 1.2$, $l = 16$, $l_1 = 12$, $w = 3$, $w_1 = 2$. (All dimensions in mm). (b) Comparison of S parameters and GD between the equivalent circuit model and the EM simulation model of proposed pulse shaped stub loaded NGDC.

and a 0.4mm broad pulse-shaped stub is inscribed to enable NGD characteristics at a single frequency band centred at 2.73 GHz. The length of the pulse-shaped stub decides the resonant frequency. This proposed circuit is simulated in a 3D EM simulator tool, and Fig. 1(b) shows its obtained S parameters and GD characteristics.

A parallel RLC resonator network models the proposed NGDC wherein R, C, and L denote self-resistance, self-capacitance, and self-inductance, respectively. The element values are extracted using the standard equations [20] given below. The magnitude of the transmission coefficient $|S_{21}|$ at the resonant frequency (f) is given by,

$$|S_{21}| = \frac{2Z_0}{Z_0 + R} \tag{1}$$

where Z_0 is the characteristic impedance of $50\,\Omega$.

From Eq. (1), the value of R can be extracted. To obtain the value of C, we use the expression for the absolute value of GD (τ), which is given as,

$$|\tau| = \frac{2R^2C}{2Z_0 + R} \tag{2}$$

Finally, the inductance value, L, is derived from

$$f = \frac{1}{2\pi\sqrt{LC}} \tag{3}$$

From the simulated results, it can be deduced that the circuit resonates at 2.736 GHz with $|S_{21}| = 16.5\,\text{dB}$ and $GD = -4.8\,\text{ns}$. The equivalent circuit parameters are extracted as $R = 646.6\,\Omega$, $C = 4.316\,\text{pF}$, and $L = 0.784\,\text{nH}$, which is further verified in a circuit simulator. The obtained S parameters and GD are plotted in Fig. 1(b) and agree well with EM simulations.

2.1. Tunable Pulse-Shaped Stub-Loaded NGDC

The group delay of a circuit is a function of the resistor, R, as shown in Eq. (2). Hence, to incorporate the GD tunability feature in the proposed NGDC, a variable resistor R_{ext} is connected at the end of the pulse-shaped stub, shown in Fig. 2(a). This proposed circuit is simulated, and its S parameters and
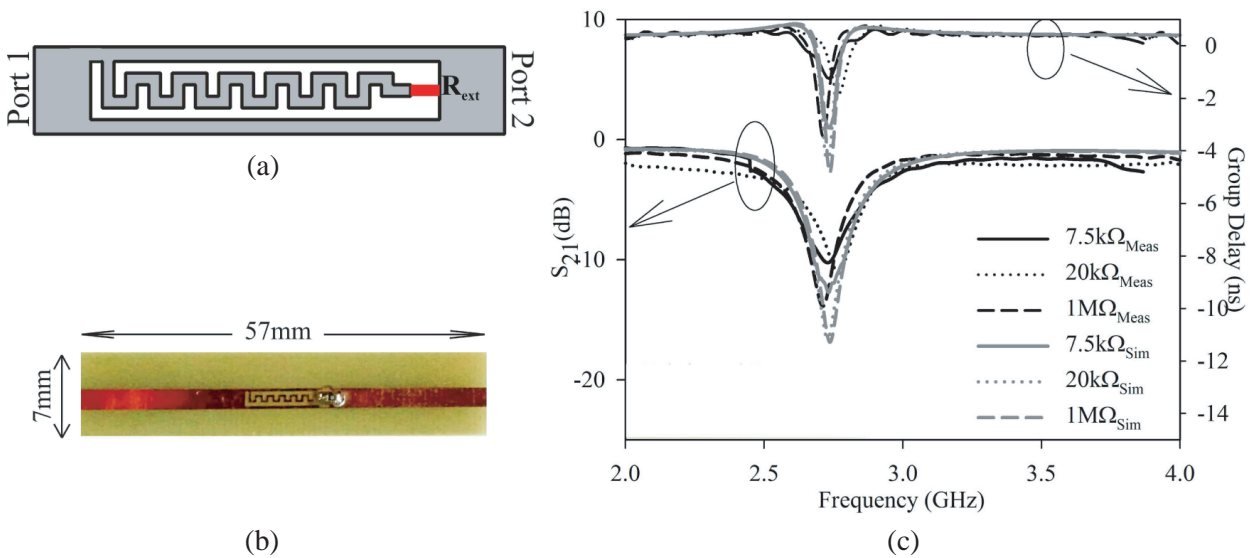
Figure 2. (a) Tunable pulse-shaped stub loaded NGDC. (b) Fabricated prototype. (c) EM simulated and measured S_{21} and GD of the proposed tunable pulse-shaped stub loaded NGDC for different values of R_{ext}.

GD characteristics are plotted in Fig. 2(c). Simulations indicate that the GD varies from 0 to -4.8 ns as the resistance changes from $1\,\text{k}\Omega$ to $1\,\text{M}\Omega$ along with an increase in signal attenuation. A marginal decrease in the bandwidth can also be observed from 130 MHz to 105 MHz which could be attributed to the increase in quality factor, Q, defined for an RLC resonator as $Q = R\sqrt{C/L}$. The simulations show that for an $R_{ext} = 1\,\text{M}\Omega$, a GD of -4.8 ns with 105 MHz NGD bandwidth is observed at 2.73 GHz.

The proposed tunable pulse-shaped stub-loaded NGDC is fabricated as shown in Fig. 2(b) and measured using a Network Analyzer. The simulated and measured group delays and their signal attenuation characteristics are plotted in Fig. 2(c). As the resistance increases from $1\,\text{k}\Omega$ to $1\,\text{M}\Omega$, the measured GD decreases from -0.5 ns to -3.5 ns. Hence, the measured results confirm the simulated tuning properties of the NGDC.

The equivalent model of this proposed tunable network is again a parallel RLC network with an additional variable resistor, R_{ext} connected in shunt, as shown in bold lines in Fig. 3. For $R_{ext} = 1\,\text{M}\Omega$, the required values are extracted from the EM simulation and substituted in Eq. (1)–Eq. (3) to obtain the circuit parameters ($R_{ext} = 1\,\text{M}\Omega$, $R = 646.8\,\Omega$, $C = 4.316\,\text{pF}$, and $L = 0.784\,\text{nH}$). The equivalent circuit model simulations confirm the EM simulated and measured results.
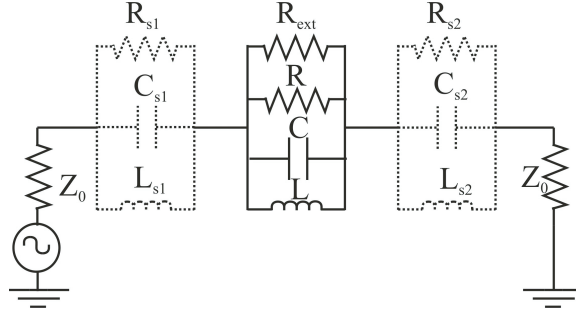
Figure 3. General equivalent circuit model of the proposed NGDCs.

2.2. Frequency Switchable and Tunable Pulse-Shaped Stub-Loaded NGDC

To further incorporate the frequency reconfigurable behaviour, two switchable stubs are added to the proposed tunable pulse-shaped stub-loaded NGDC design, as shown in Fig. 4(a). S_1 and S_2 are RF switches, and the proposed modified circuit operates for multiple frequency bands depending on the switching states of S_1 and S_2. Similar to the previous design, this circuit is implemented on an FR4 substrate with a 4.7 dielectric constant and 1.6 mm height. The simulated S parameters and GD for $S_1 = S_2 = \text{OFF}$ and $R_{ext} = 1\,\text{M}\Omega$ are plotted in Fig. 4(b). These simulation results validate its multi-band property with resonant frequencies at 1.98 and 3 GHz. The circuit in Fig. 3 is equivalent to this proposed circuit wherein the resonator structure having elements R, R_{ext}, L, and C models the resistor-loaded pulse-shaped stub and the two resonators with the elements R_{Si}, C_{Si}, and L_{Si} model the two outer stubs. Here $i = 1$ and 2 correspond to the stub at the top and bottom, respectively.

For $S_1 = S_2 = \text{ON}$, the two outer stubs will be of identical length, as shown in Fig. 5(b)(i), and the circuit resonates at 2.91/3.73 GHz with S_{21} of $-17.48/-24.75$ dB and GD of $-3.17/-2.67$ ns respectively. Since the outer stubs are of equal length, the two corresponding resonators have the same values and resonate at the same frequency of 3.73 GHz. The resonance at 2.91 GHz, however, corresponds to the pulse-shaped stub with R_{ext}. These are further confirmed from the electric field distribution of the circuit shown in Fig. 5(b)(i). Now, as we turn OFF S_2, the stub length at the bottom almost doubles as compared to that of the stub at the top, as shown in Fig. 5(b)(ii). Hence, the circuit resonates at three different frequencies 2.12/2.96/3.46 GHz with S_{21} of $-14.4/-15.5/-22.5$ dB and GD of $-3.63/-3.43/-3.6$ ns, respectively. As we toggle the switching states of S_1 to OFF and S_2 to ON, the stub length increases at the top and decreases at the bottom, as shown in Fig. 5(b)(iii). As a result, the circuit resonates at almost similar frequencies in the previous scenario. Finally, when both S_1 and S_2 are in the OFF state, the stubs are of equal span with longer dimensions, as shown in Fig. 5(b)(iv). Therefore, the circuit resonates at two lower frequencies of 1.98/3 GHz with S_{21} of $-20.5/-17.5$ dB and GD of $-4.59/-4.53$ ns, respectively.

(a)

(b)
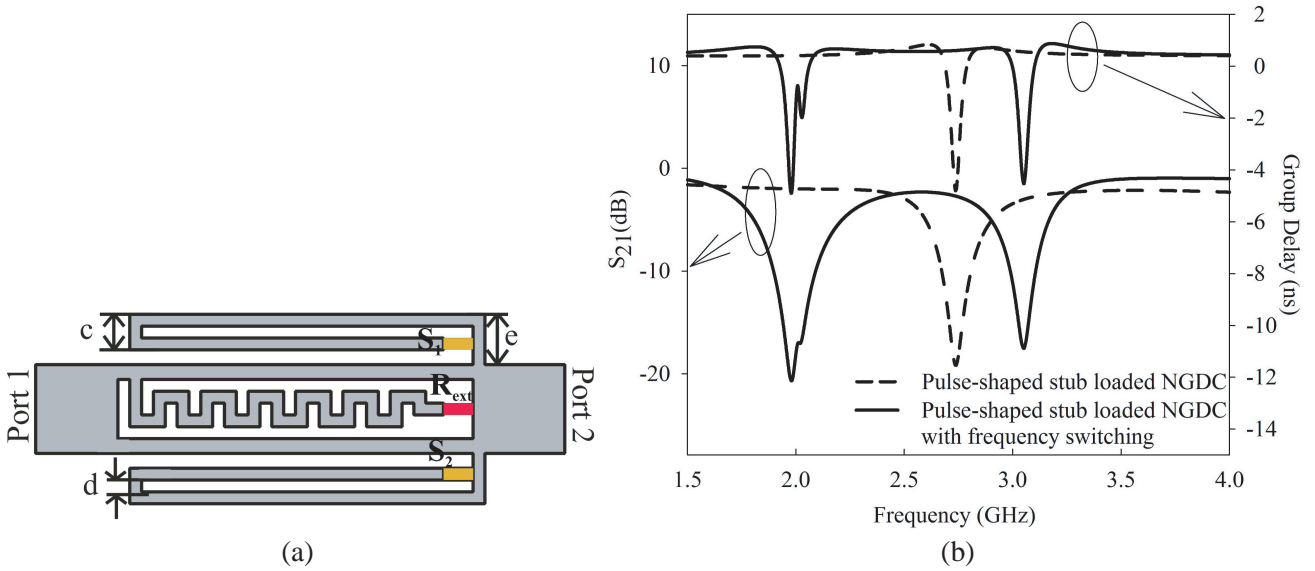
Figure 4. (a) Frequency switchable and tunable pulse-shaped stub-loaded NGDC — $c = 1$, $d = 0.3$, and $e = 1.8$. (All dimensions in mm), (b) S_{21} and GD of pulse-shaped stub loaded NGDC and pulse-shaped stub loaded NGDC with frequency switching.

As previously discussed, the equivalent circuit parameters for all the switching conditions of S_1 and S_2 are extracted with the aid of Eq. (1)–Eq. (3) and are summarised in Table 1. Using these parameters, the equivalent circuit model simulations are carried out in a circuit simulator tool, and the obtained GD characteristics are compared with those of EM simulation, as shown in Fig. 5(a). It shows that the equivalent circuit model simulations agree well with EM simulations. During all the simulations, the resistor R_{ext} is fixed at $1\,\text{M}\Omega$.

Table 1. Equivalent circuit parameters of different switching conditions of S_1 and S_2.

S_1	S_2	R_{S1} Ohms	C_{S1} pF	L_{S1} nH	R Ohms	C pF	L nH	R_{S2} Ohms	C_{S2} pF	L_{S2} nH
ON	ON	1.688 k	0.842	2.16	699	2.53	1.18	1.688 k	0.842	2.16
ON	OFF	475	4.62	1.22	544	3.734	0.77	1.3 k	1.49	1.42
OFF	ON	500	4.67	1.2	505	4.058	0.72	1.28 k	1.52	1.35
OFF	OFF	1.01 k	2.486	2.59	702	3.68	0.738	1.01 k	2.486	2.59

The proposed design is fabricated, and metal strips are used to emulate the RF switch in its ON state. Fig. 5(a) plots the measurements taken and depicts the operational frequencies achieved with this circuit at different states of S_1 and S_2. The group delay tunability is also achieved by varying R_{ext} from $1\,\text{k}\Omega$ to $1\,\text{M}\Omega$ for each value of S_1 and S_2. Hence, these results confirm the frequency switchability and GD tunability achieved during simulations. The discrepancies between the measured and simulated data in centre frequencies and group delays could be primarily due to fabrication uncertainties. However, the measured results substantiate the novel ideas presented by the simulated results.
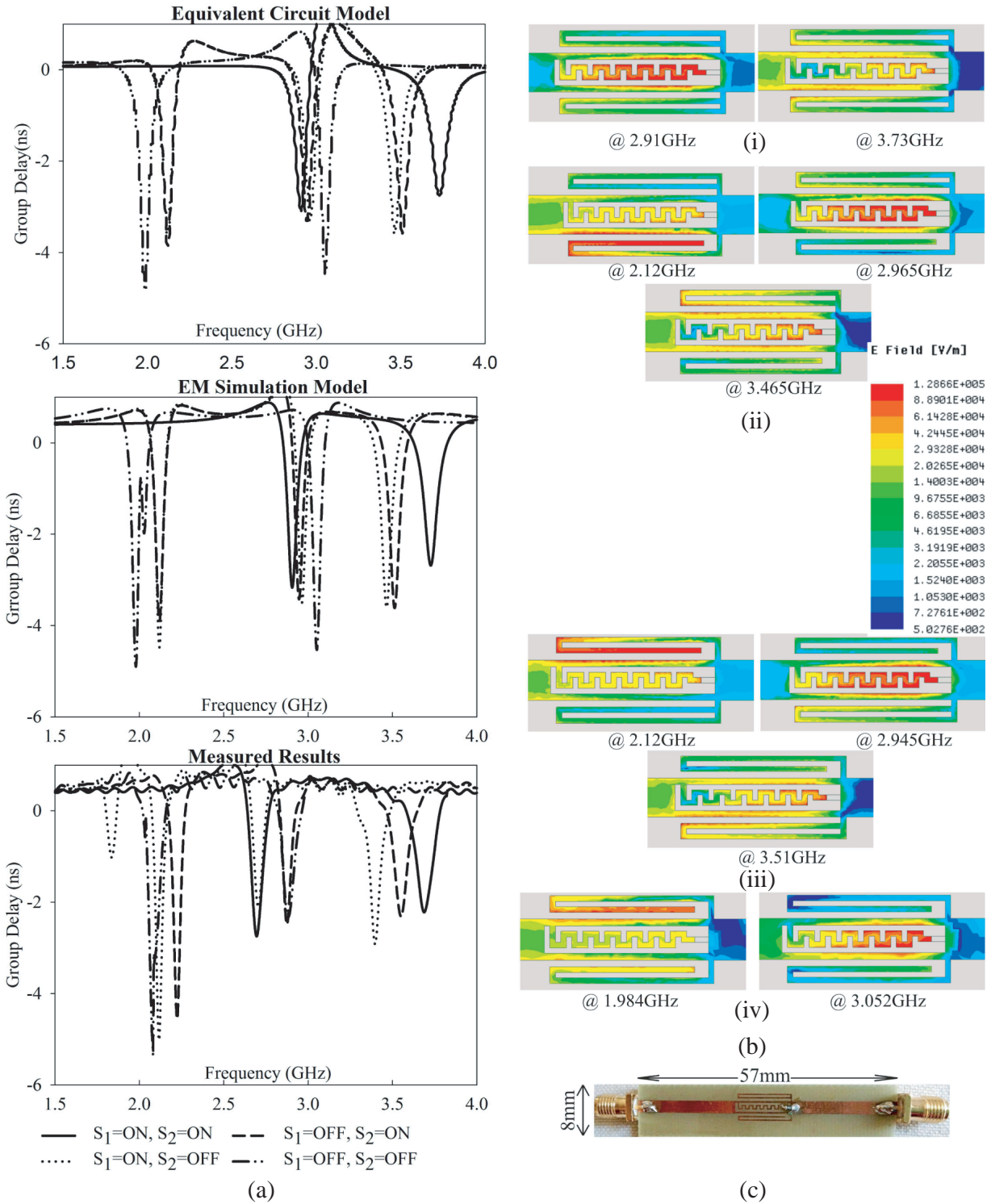
Figure 5. (a) GD characteristics from equivalent circuit model, EM simulation model and measurements of the proposed pulse-shaped stub loaded NGDC with frequency switchability. (b) Electric field distribution of the proposed tunable pulse-shaped stub-loaded NGDC with frequency switchability for different states of switches S_1 and S_2 — (i) $S_1 = $ ON, $S_2 = $ ON, (ii) $S_1 = $ ON, $S_2 = $ OFF, (iii) $S_1 = $ OFF, $S_2 = $ ON and (iv) $S_1 = $ OFF, $S_2 = $ OFF. (c) Fabricated prototype.

3. COMPACT AND TUNABLE U-SHAPED STUBS-LOADED NGDC WITH FREQUENCY SWITCHABILITY

A compact NGDC design incorporating variable resistance and switching within the $50\,\Omega$ microstrip line is further proposed and shown in Fig. 6(a). Two U-shaped stubs are inscribed inside the defection to generate NGD at multiple frequencies. The circuit is implemented on an FR4 substrate. The results plotted in Fig. 6(b) show that the circuit has two resonant frequencies wherein the stub with the resistor M_R is the reason for the first resonance (lower frequency band), and the stub with the switch M_S causes the second resonance. Figs. 7(a), (b), (c), and (d) show the proposed circuit's electric field distributions for the two switching conditions of M_S with M_R varying from $1\,k\Omega$ to $1\,M\Omega$.
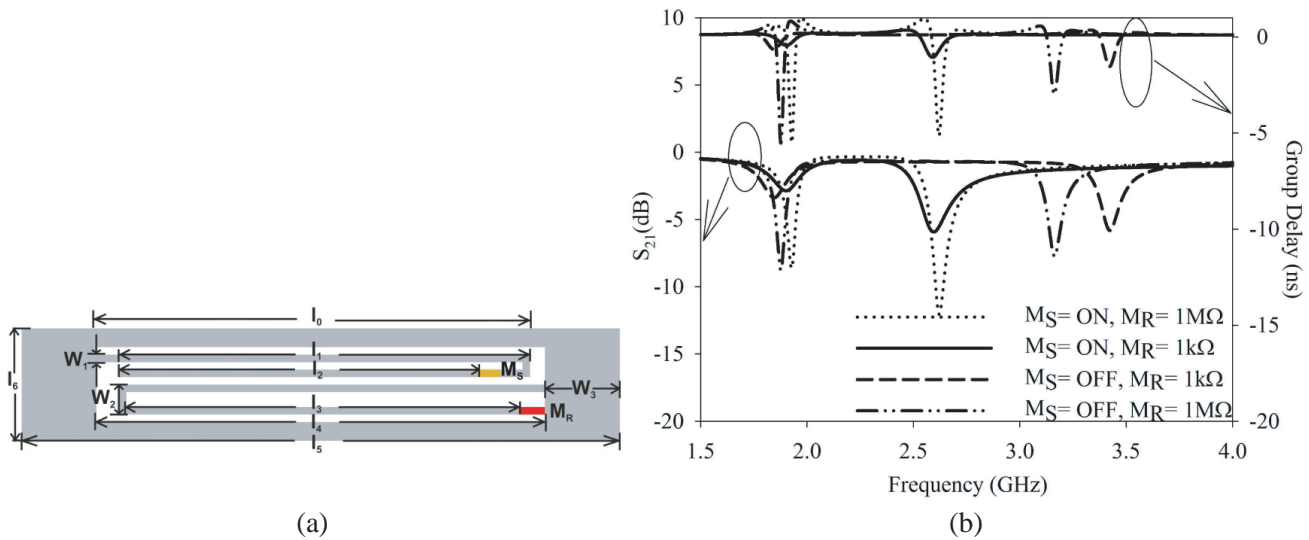
Figure 6. (a) Tunable U-shaped stubs loaded NGDC with frequency switchability. $l_0 = 11.6$, $l_1 = 11$, $l_2 = 9.6$, $l_3 = 10.5$, $l_4 = 12$, $l_5 = 14$, $l_6 = 3$, $W_1 = 0.2$, $W_2 = 0.8$, $W_3 = 1$. All units of length are in millimetre (mm). (b) S parameters and GD of the proposed U-shaped stub loaded NGDC.

When M_S is in the ON state, and M_R is $1\,k\Omega$, a group delay of $-0.4/-1.1\,ns$ is obtained at $1.9/2.6\text{v}GHz$, respectively. As observed in the previous designs, as M_R increases, the GD decreases; hence, for $M_R = 1\,M\Omega$, the GD decreases from $-0.4\,ns$ to $-5.5\,ns$ at $1.9\,GHz$ and $-1.1\,ns$ to $-5.2\,ns$ at $2.6\,GHz$. As we change the state of M_S to the OFF state, the length of the U stub decreases (l_2 disconnects from the l_1 strip), and the operating frequency shifts to the higher frequency band. Thus, when M_S is turned OFF and $M_R = 1\,k\Omega$, the first resonant frequency remains at $1.9\,GHz$ with a GD of $-0.6\,ns$, and the second resonant frequency shifts from $2.6\,GHz$ to $3.4\,GHz$ with a GD of $-1.5\,ns$. Then, as we increase the resistance of M_R to $1\,M\Omega$, the circuit generates much lower GD of $-5.5\,ns$ and $-3\,ns$ at 1.9 and $3.2\,GHz$, respectively. The results show that there is a slight frequency shift from $3.2\,GHz$ to $3.4\,GHz$ as we fix the M_S at its OFF state and vary M_R from $1\,M\Omega$ to $1\,k\Omega$. This is primarily due to the field coupling to the l_2 strip from the neighbouring stubs, as shown in Figs. 7(c) and (d).

We can change the operating frequency as per our requirements by accurately selecting the required stub length and adding multiple switches. Thus, for $M_S = OFF$ and $M_R = 1\,M\Omega$, the proposed tunable U-shaped stubs loaded NGD circuit has an NGD bandwidth of $49\,MHz$ and $77\,MHz$ at its two resonant frequencies. Meanwhile, for $M_S = ON$ and $M_R = 1\,M\Omega$, the circuit has NGD bandwidths of $42\,MHz$ and $84\,MHz$ at its resonances. Compared to the proposed pulse-shaped stub-loaded circuits, the U-shaped stubs-loaded NGDC has a more compact design but lower NGD bandwidth since it has thinner stub width of $0.2\,mm$. Cascading the two U-shaped stubs loaded NGDCs will increase the NGD bandwidth if required.

Table 2 summarises various NGDCs available in the literature so far and compares them in terms

of centre frequency, group delay, S_{21} and S_{11} at the peak of NGD, NGD bandwidth, tunability, and size. Our proposed designs are implemented on a $50\,\Omega$ microstrip line, making them compact compared to the other circuits. In addition, NGD tunability and multi-band frequency switching capability are achieved with the aid of variable resistors and RF switches. NGD BW in this paper is the entire bandwidth over which the group delay is negative. At the same time, this achieved bandwidth is well within the 3-dB variations from the minimum of S_{21} for all the proposed works. Therefore, NGD BW within the $3\,\mathrm{dB}$ variations from S_{21} minimum is calculated and summarised for our proposed works in Table 2. Hence, distortion appearing at the output pulse will not occur as mentioned in [30]. However, the signal attenuation caused by NGD generation remains a problem. Since signal attenuation is a necessary loss for NGD, these designs confirm the tradeoff between NGD and signal attenuation as reported in literature [25, 31]. Moreover, general-purpose gain amplifiers can compensate for this attenuation. The reflection losses in our designs can be compensated by using 90° hybrid couplers or power dividers, and combiners [25, 29].

Table 2. Comparison with similar reported in the literature.

Ref. (year)	Centre Frequency (GHz)	GD_{MAX} (ns)	S_{21} (dB)	S_{11} (dB)	NGD BW (GD ≤ 0 ns) (MHz)	Tunability	Size (mm × mm)	NGD BW (Within 3 dB)
[23] (2014)	3.5/5.15	$-4.54/-4.2$	$-47/-39$	-	58/60	No	-	-
[24] (2015)	3.44/ 4.91	$-4.5/-4.5$	$-21/-23$	-	-	No	20×8	-
[20] (2019)	2.8/4.3 /5.8	$-6.5/-5.4$ $/-3.0$	$-21/-24$ $/-23$	-	120/180 /250	GD	30×2.46	-
[25] (2020)	1.2	-2.8	-2.2	-15	30	No	64×12	-
[26] (2014)	1.96	-6.5	-21.2	-24	90	No	70×70	-
[27] (2021)	1.2/3.5 /5.8	$-1.1/-1.2$ $/-1.1$	$-16/-25$ $/-19$	$-16/-17$ $/-16$	-	No	20×34.5	-
[28] (2022)	1	-2.02	-6.5	-11.3	-	GD flatness	37.6×52.5	-
[29] (2014)	2.125	-8.2	-37.84	≤ -19	40	No	-	-
[31] (2021)	1.89	-1	-1.7	-15	20	No	42×87	-
Work[1]	2.7	-3.5	-17	-3	105	GD	57×7	56
Work[2]	2.1/3.1	$-4.6/-4.5$	$-20/-17$	$-1/-3$	155/120	GD, Freq	57×8	60/60
	2.1/2.9 /3.5	$-3.5/-3.4$ $-/3.6$	$-15/-13$ $/-18$	$-2/-3$ $/-1$	100/100 /150/110			65/75 /75
	2.1/3 /3.6	$-3.6/-3.1$ $/-3.5$	$-14/-14$ $/-13$	$-2/-3$ $/-2$	100/105 /155			65/70 /70
	2.9/3.72	$-3.1/-2.68$	$-17/-24$	$-3/-2$	110/195			75/90
Work[3]	1.87/3.2	$-5.47/-3$	$-9/-4$	$-6/-4$	49/77	GD, Freq	14×4	42/49
	1.93/2.62	$-5.5/-5.2$	$-8/-12$	$-5/-2$	42/84			42/ 60

1: Tunable pulse-shaped stubs-loaded NGDC

2: Tunable pulse-shaped stubs-loaded NGDC with frequency switchability

3: Compact and tunable U-shaped stubs-loaded NGDC with frequency switchability
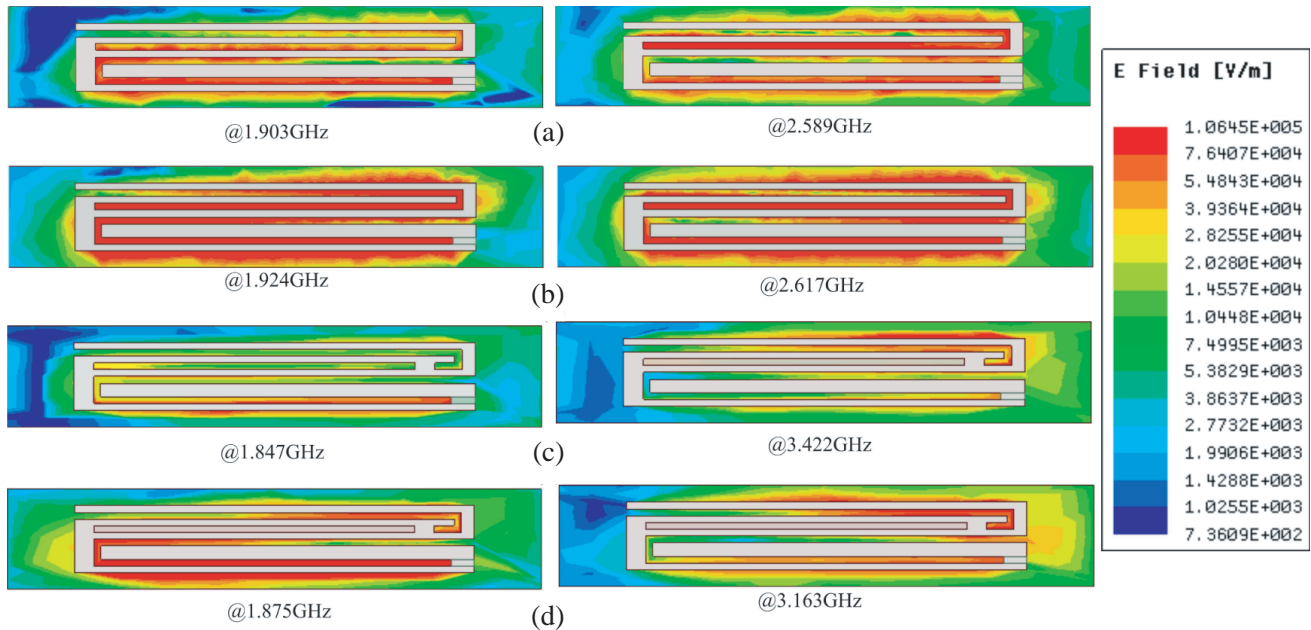
Figure 7. Electric field distribution of the proposed U-shaped stubs loaded NGDC for different switching states of M_S and $M_R = 1\,\mathrm{k\Omega}/1\,\mathrm{M\Omega}$. (a) $M_S = $ ON and $M_R = 1\,\mathrm{k\Omega}$. (b) $M_S = $ ON and $M_R = 1\,\mathrm{M\Omega}$. (c) $M_S = $ OFF and $M_R = 1\,\mathrm{k\Omega}$. (d) $M_S = $ OFF and $M_R = 1\,\mathrm{M\Omega}$.

4. CONCLUSION

In this paper, we have presented three tunable NGDCs based on defected microstrip structures, implemented on $50\,\Omega$ microstrip lines, making them compact compared to the reported available circuits. Firstly, a pulse-shaped stub-loaded NGDC with group delay tunability is designed and fabricated wherein we connected a variable resistor across a slot, enabling NGD tuning. Then, two switchable stubs are appended to the circuit to add the reconfigurable multi-band feature, which constitutes the second NGDC design. The measured results confirm the performance. Finally, a more compact, switchable multi-band and tunable NGDC is proposed where two U-shaped switchable stubs are inscribed inside a $50\,\Omega$ microstrip line. The variable resistor in the inverted U structure controls its signal attenuation and enables NGD tuning. The RF switch in the circuit allowed the switchable multi-band feature. All our three proposed works are further confirmed by their equivalent circuit model design analysis.

ACKNOWLEDGMENT

REFERENCES

1. Su, Y. U., "Group delay variations in microwave filters and equalization methodologies," Department of Microtechnology and Nanoscience, Master's Thesis in Microtechnology and Nanoscience, 2012.

2. Xiao, J. K., Q. F. Wang, and J. G. Ma, "Negative group delay circuits and applications: Feedforward amplifiers, phased-array antennas, constant phase shifters, non-foster elements, interconnection equalization, and power dividers", *IEEE Microwave Magazine*, Vol. 22, No. 2, 16–32, 2021.

3. Choi, H., G. Chaudhary, T. Moon, Y. Jeong, J. Lim, and C. D. Kim, "A design of composite negative group delay circuit with lower signal attenuation for performance improvement of power amplifier linearization techniques," *IEEE MTT-S Int. Microw. Symp. Dig.*, 1–4, Jun. 2011.

4. Choi, H., Y. Kim, Y. Jeong, and J. Lim, "A design of size-reduced negative group delay circuit using a stepped impedance resonator," *Proc. Asia-Pacific Microw. Conf.*, 118–1121, Dec. 2010.

5. Kitano, M., T. Nakanishi, and K. Sugiyama, "Negative group delay and superluminal propagation: An electronic circuit approach," *IEEE Journal of Selected Topics in Quantum Electronics*, Vol. 9, No. 1, 43–51, Jan.–Feb. 2003.

6. Brillouin, L., *Wave Propagation and Group Velocity*, Academic, Cambridge, MA, USA, 1960.

7. Choi, H., Y. Jeong, C. D. Kim, and J. S. Kenney, "Efficiency enhancement of feed forward amplifiers by employing a negative group-delay circuit," *IEEE Trans. Microw. Theory Techn.*, Vol. 58, No. 5, 1116–1125, May 2010.

8. Oh, S. S. and L. Shafai, "Compensated circuit with characteristics of lossless double negative materials and its application to array antennas," *IET Microw. Antennas Propag.*, Vol. 1, No. 1, 29–38, 2007.

9. Shao, T., Z. Wang, S. Fang, H. Liu, and Z. N. Chen, "A full-passband linear-phase band-pass filter equalized with negative group delay circuits," *IEEE Access*, Vol. 8, 43336–43343, 2020.

10. Choi, H., Y. Jeong, C. D. Kim, and J. S. Kenney, "Bandwidth enhancement of an analog feedback amplifier by employing a negative group delay circuit," *Progress In Electromagnetics Research*, Vol. 105, 253–272, 2010.

11. Ravelo, B. E. G., A. Pérennec, and M. Le Roy, "Synthesis of frequency-independent phase shifters using negative group delay active circuit," *International Journal of RF and Microwave Computer-Aided Engineering*, Vol. 21, No. 1, 17–24, Wiley, 2011.

12. Ravelo, B., M. Le Roy, and A. Pérennec, "Application of negative group delay active circuits to the design of broadband and constant phase shifters," *Microw. Opt. Technol. Lett.*, Vol. 50, 3078–3080, 2008.

13. Wan, F., et al., "Design of multi-scale negative group delay circuit for sensors signal time-delay cancellation," *IEEE Sensors J.*, Vol. 19, No. 19, 8951–9962, 2019.

14. Ravelo, B., "Similitude between the NGD function and filter gain behaviours," *Int. J. Circ. Theor. Appl.*, Vol. 42, No. 10, 1016–1032, Oct. 2014.

15. Chaudhary, G., Y. Jeong, and J. Lim, "Miniaturized negative group delay circuit using defected microstrip structure and lumped elements," *2013 IEEE MTT-S International Microwave Symposium Digest (MTT)*, 1–3, 2013.

16. Choi, H., et al., "A compact DGS load-network for highly efficient class-E power amplifir," *2009 European Microwave Conference (EuMC)*, 492–495, 2009.

17. Radisic, V., et al., "Novel 2-d photonic bandgap structure for microstrip lines," *IEEE Microwave and Guided Wave Letters*, Vol. 8, No. 2, 69–71, 1998.

18. Kandic, M. and G. E. Bridges, "Asymptotic limits of negative group delay in active resonator-based distributed circuits," *IEEE Transactions on Circuits and Systems I: Regular Papers*, Vol. 58, No. 8, 1727–1735, Aug. 2011.

19. Chaudhary, G., Y. Jeong, and J. Lim, "Microstrip line negative group delay filters for microwave circuits," *IEEE Trans. Microw. Theory Techn.*, Vol. 62, No. 2, 234–243, Feb. 2014.

20. Xiao, J.-K. and Q.-F. Wang, "Individually controllable tri-band negative group delay circuit using defected microstrip structure," *2019 Cross Strait Quad-Regional Radio Science and Wireless Technology Conference (CSQRWC)*, 1–3, 2019.

21. Zhao, G. and B. You, "A tunable negative group delay filter using memristors," *2020 IEEE MTT-S International Wireless Symposium (IWS)*, Shanghai, China, 2020.

22. Palson, C. L., R. K. Sreelal, D. D. Krishna, and B. R. Jose, "Memristor based tunable negative group delay circuit," *2021 International Conference on Advances in Computing and Communications (ICACC)*, 1–4, 2021.

23. Chaudhary, G., Y. Jeong, and J. Lim, "Miniaturized dual-band negative group delay circuit using dual-plane defected structures," *IEEE Microwave and Wireless Components Letters*, Vol. 24, No. 8, 521–523, Aug. 2014.

24. Chaudhary, G., P. Kim, J. Jeong, Y. Jeong, and J. Lim, "Dual-band negative group delay circuit using defected microstrip structure," *2015 IEEE Radio and Wireless Symposium (RWS)*, 129–131, 2015.

25. Wan, F., N. Li, B. Ravelo, and J. Ge, "O=O shape low-loss negative group delay microstrip circuit," *IEEE Transactions on Circuits and Systems II: Express Briefs*, Vol. 67, No. 10, 1795–1799, Oct. 2020.

26. Chaudhary, G., Y. Jeong, and J. Lim, "Microstrip line negative group delay filters for microwave circuits," *IEEE Transactions on Microwave Theory and Techniques*, Vol. 62, No. 2, 234–243, Feb. 2014.

27. Meng, Y., Z. Wang, S.-J. Fang, and H. Liu, "A tri-band negative group delay circuit for multiband wireless applications," *Progress In Electromagnetics Research C*, Vol. 108, 159–169, 2021.

28. Meng, Y., Z. Wang, S. Fang, and H. Liu, "Reconfigurable negative group delay circuit with tunable group delay flatness," *Int. J. RF Microw. Comput. Aided Eng.*, Vol. 32, No. 6, e23159, 2022.

29. Chaudhary, G., Y. Jeong, and J. Lim, "Realization of negative group delay network using defected microstrip structure," *International Journal of Antennas and Propogation*, Vol. 2014, 1–5, 2014.

30. Kandic, M. and G. Bridges, "Negative group delay prototype filter based on cascaded second order stages implemented with Sallen-Key topology," *Progress In Electromagnetics Research B*, Vol. 94, 1–18, Sep. 2021.

31. Wan, F., N. Li, B. Ravelo, W. Rahajandraibe, and S. Lalléchère, "Design of shape stub-based negative group delay circuit," *IEEE Design & Test*, Vol. 38, No. 2, 78–88, Apr. 2021.